Graphene on nickel (100) micrograins: modulating the interface interaction by extended moiré superstructures

1. Single- and poly-crystalline substrate characterization

For the characterization of the single- and poly-crystalline substrate it is useful to remind that the crystalline structure of Ni is face-centered cubic and its bulk lattice constant, a_{bulk}, is 3.52 Å, which determine the periodicity of a selected surface and the relevant parameters, i.e., in-plane lattice constant and interplanar distances.

1.1 Atomic structure and characterization of a single crystalline Ni(100) surface

The (100) surface is described by a square lattice with parameter $a_{Ni}= \sqrt{2}/2\ a_{bulk}$ =2.49 Å (figure S1). The interplanar distance characterizing the {100} family of planes is 1/2 a_{bulk} = 1.76 Å. For comparison, 2.49 Å, and 2.03 Å are the interplanar distances in the other low Miller indices families of planes, {110} and {111}, respectively, corresponding to $\sqrt{2}/2\ a_{bulk}$ and $\sqrt{3}/3\ a_{bulk}$.

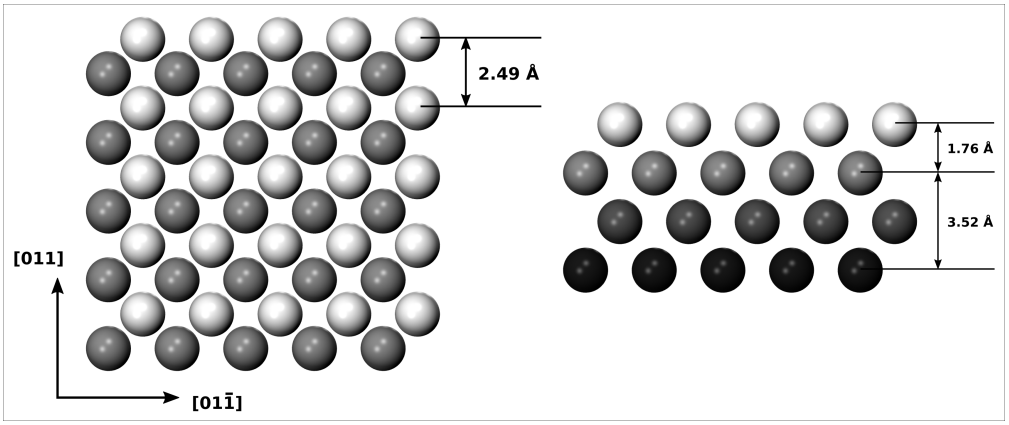

Figure S1 Stick-and-ball model of Ni(100) surface. **Left:** top view, where the topmost atoms (white) form a square lattice shifted with respect to the one formed by the second layer of Ni atoms (grey). [011] and [01$\bar{1}$] directions are denoted by arrows. **Right:** side view of the model, where the stacking of the atomic planes parallel to the surface is rendered by using different grey tones.

A line profile (see figure S2) along the (100) single crystal surface clearly indicates the presence of mono and biatomic steps, since the height differences correspond to one and two interplanar distances in the {100} family of planes, respectively.

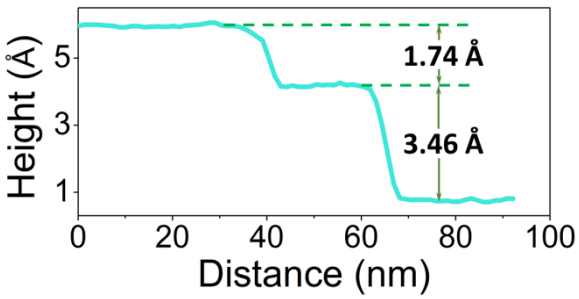

Figure S2 Line profile along the white line in figure 1(a) across two consecutive steps on the single crystal surface. From the height it is evident that the steps correspond to one and two atomic planes, respectively (see side view in figure S1).

1.2 Characterizations of the polycrystalline nickel foil

The polycrystalline Ni foil (see figure S3) exhibits different facets. X-ray diffractograms (XRD) show that, after per-treatment, the (100) and (111) facets are the most common ones (see figure S4). The surface lattice symmetry of a selected facet can be visualized by STM (see figure S5). The analysis of the step height distribution on a given grain (see figure S6) confirm the orientation of the facet.

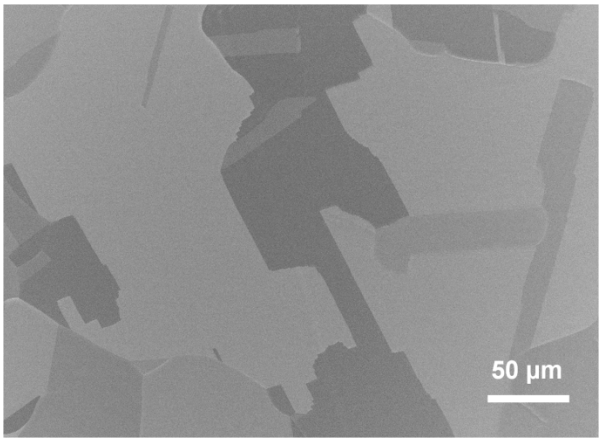

Figure S3 Scanning electron microscope (SEM) image of the polycrystalline Ni surface after pretreatment procedures. The pre-processing of the surface includes mechanical polishing, rinse with DI water and organic solvents, hydrogen annealing in CVD furnace and sputtering-and-annealing cycles in UHV chamber (see Methods for more details). The grain sizes can be evaluated from the uniform-contrast area in the image.

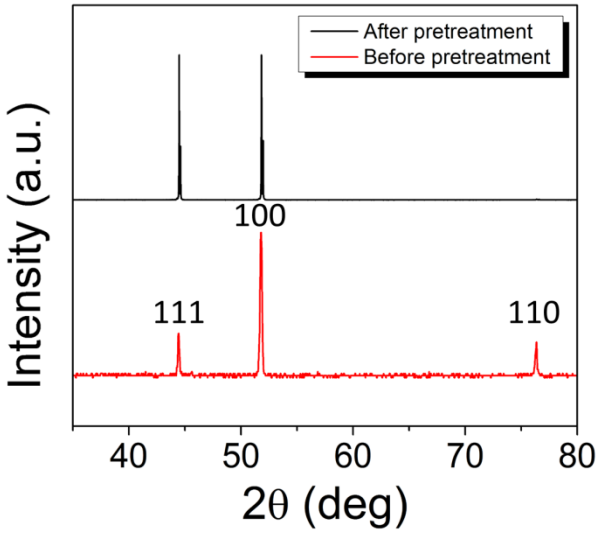

Figure S4 X-ray diffractograms (XRD) of polycrystalline Ni foil before (red) and after (black) pre-treatment. It can be seen that the FWHMs of (111) and (100) peaks become sharper after pre-treatment.

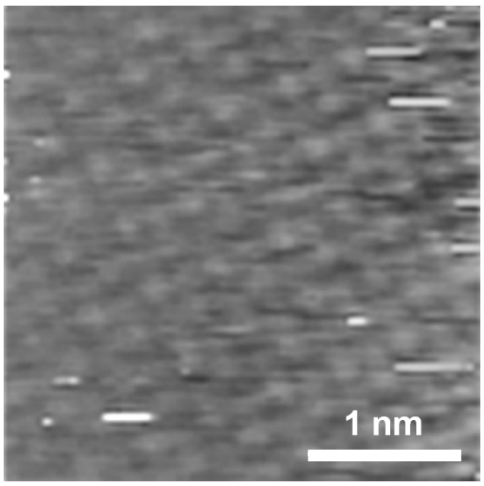

Figure S5 STM image [0.01 V, 9.25 nA] taken on the selected facet, in which the square symmetry of the atomic arrangement can be identified.

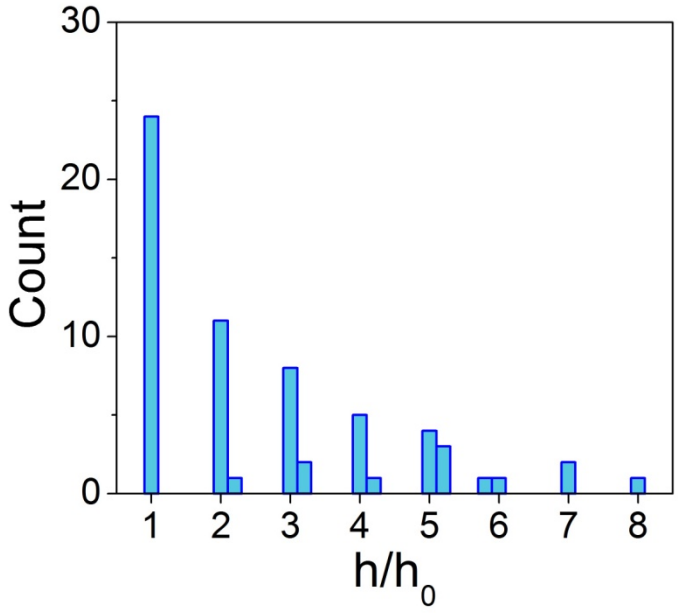

Figure S6 Histogram of the step height distribution for the selected (100) facets of the polycrystalline Ni foil. h_0, the monatomic step height on Ni(100) is adopted as a benchmark to evaluate the measured step height (h). The values of h/h_0 turn out to be always around integers (1, 2, 3…), indicating that the steps correspond to single or multiple atomic layers on Ni(100), confirming the orientation of the measured grain.

2. Geometrical analysis of graphene moiré superstructure

The misorientation angle ($\boldsymbol{\theta}$) between graphene and Ni(100) is herein defined as the smallest angle by which graphene needs to rotate (clock- or anticlock-wise) in order to align one of its three zigzag directions with one of the two lattice vector directions of Ni(100) surface (figure S7, left panels). For example, we consider the configuration illustrated in the right panel of figure S7: vectors $\boldsymbol{a_1}$ and $\boldsymbol{a_2}$ are along two specific high-symmetry crystallographic direction of Ni(100) surface; vectors $\boldsymbol{b_1}$ and $\boldsymbol{b_2}$ are along two zigzag directions of graphene; $\boldsymbol{\theta_1}$ and $\boldsymbol{\theta_2}$ are the relative angles between $\boldsymbol{a_i}$ and $\boldsymbol{b_i}$. In this case, since $\boldsymbol{\theta_1} < 15° < \boldsymbol{\theta_2}$, $\boldsymbol{\theta_1}$ turns out to be the smallest angle for graphene rotation to make $\boldsymbol{a_1}$ and $\boldsymbol{b_1}$ aligned, i.e. $\boldsymbol{\theta} = \boldsymbol{\theta_1}$. In fact, in view of the intrinsic symmetry of graphene and Ni(100) lattice, $\boldsymbol{\theta}$ varies only in the range of 0-15°, and no matter how graphene rotates with respect to the substrate, (only) one value of $\boldsymbol{\theta}$ exists to specifically define the relative misorientation (figures S8,9).

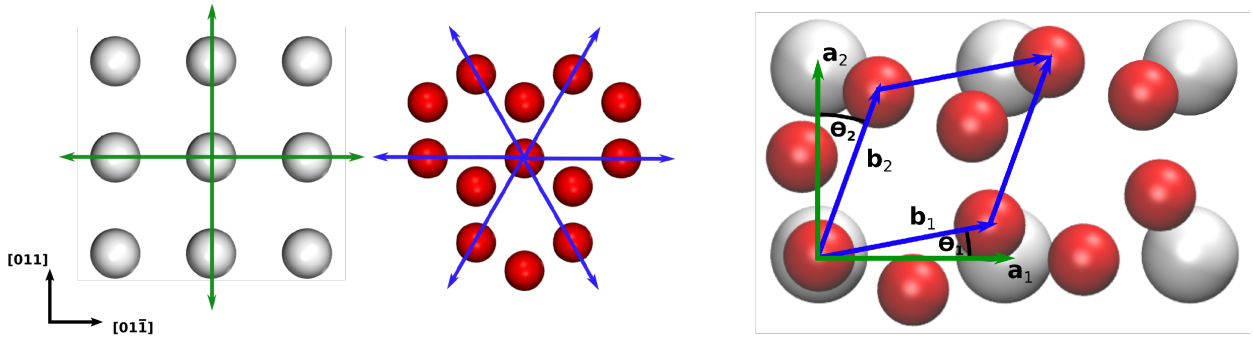

Figure S7 Lattice vectors of Ni(100) surface ($\boldsymbol{a_1}$, $\boldsymbol{a_2}$) and graphene ($\boldsymbol{b_1}$, $\boldsymbol{b_2}$), superimposed on the corresponding atomic model. The white and red spheres represent nickel atoms on (100) surface and carbon atoms in graphene, respectively. The lengths of Ni(100) and graphene lattice vectors are supposed to be 2.49 Å and 2.46 Å, respectively.

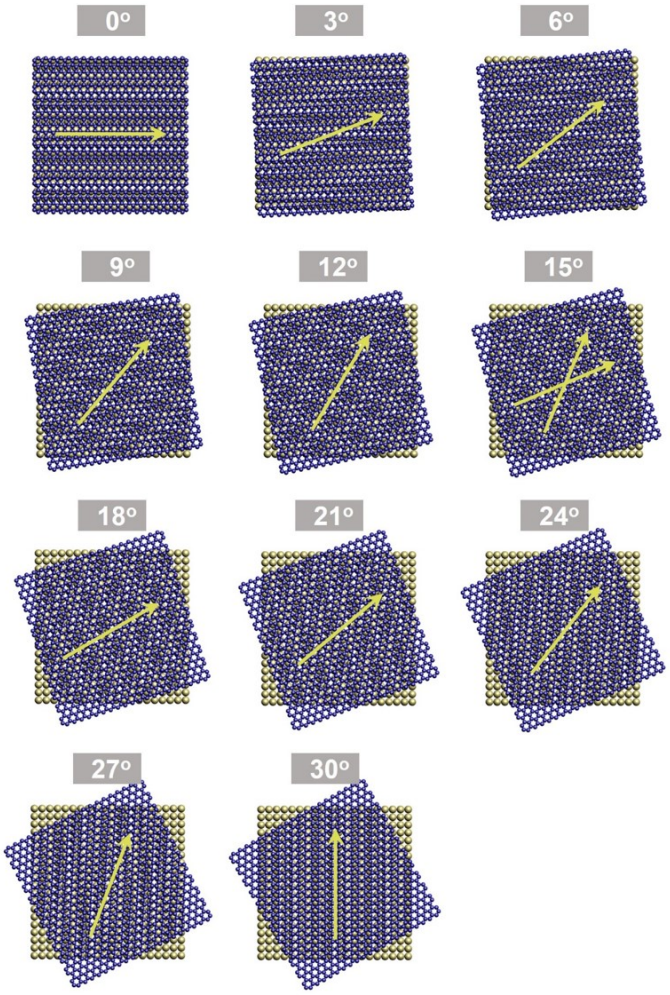

Figure S8 Schematic illustration of moiré structures with different rotation angles $\boldsymbol{\theta_1}$ between the lattice vector $\boldsymbol{a_1}$ of Ni(100) and the lattice vector $\boldsymbol{b_1}$ of graphene (see Figure S7). The yellow and blue spheres represent nickel atoms on (100) surface and carbon atoms in graphene, respectively. With the increase of $\boldsymbol{\theta_1}$ from 0^o to 15^o, the superstructure changes from a striped configuration to a rhombic network. The yellow arrow denotes the orientation of moiré pattern when the superstructure is striped or one side of the moiré supercell when the superstructure is a rhombic network. By gradually increasing the value of $\boldsymbol{\theta_1}$, the orientation marked by the yellow arrow changes in a continuous manner accordingly. When $\boldsymbol{\theta_1}$ is 15^o, the orientations marked by both the yellow arrows are equivalent. This means that at this angle the moiré super cell is an equilateral rhombus.

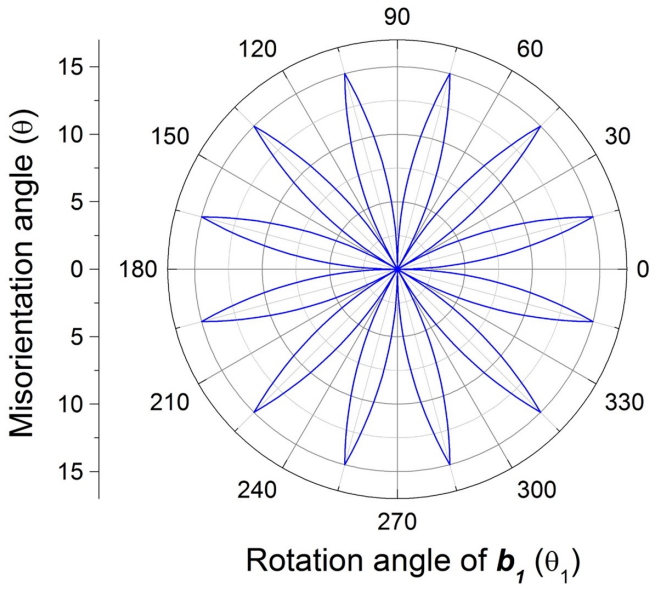

Figure S9 Polar plot illustrating the dependence of $\boldsymbol{\theta}$ on $\boldsymbol{\theta_1}$, the latter being the rotation angle of lattice vector $\boldsymbol{b_1}$ (with respect to $\boldsymbol{a_1}$). $\boldsymbol{\theta_1}$, $\boldsymbol{a_1}$, $\boldsymbol{b_1}$ are as shown in figure S7. Both $\boldsymbol{\theta}$ and $\boldsymbol{\theta_1}$ are in the unit of degree.

3. Graphene rotational domains on Ni(100) at the mesoscale

As reported in the main text, analysis of STM images indicates that the misorientation angle θ assumes only a set of discrete values in the 0° – 15° range, with predominance of 0°.

The lateral distribution of rotational domains was investigated at the mesoscale on Ni(100) with Low Energy Electron Microscopy (LEEM) and related microspot-LEED (μLEED). LEEM images of a graphene-covered surface prepared at 560˚C typically show large graphene domains characterized by dark appearance (see figure S10(a)). They correspond to graphene characterized by $\boldsymbol{\theta} = 0^{\circ}$, as indicated by the μLEED pattern shown in figure S10(b), which does not vary on the whole area, proving that the latter is very homogeneous over a lateral extent of several microns. μLEED also indicates that the brighter areas in figure S10(a) correspond instead to a mixture of small domains with different rotation angles, characterized by similar electron reflectivity and thus indistinguishable in LEEM.

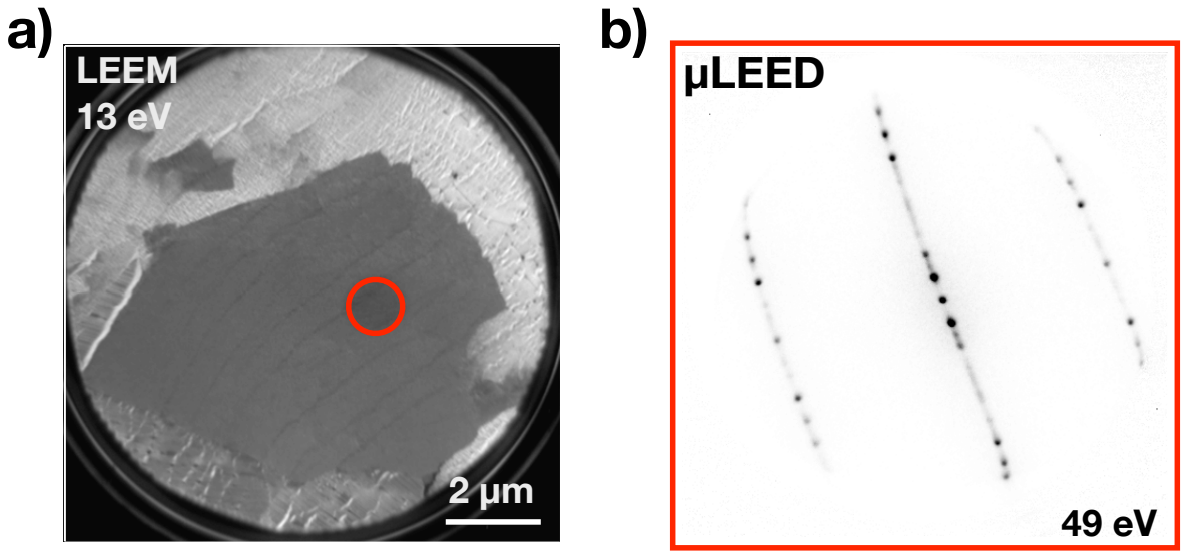

Figure S10 (a) LEEM image of a graphene region presenting a graphene flake (in dark grey) about 10 µm wide and a surrounding brighter region. (b) Microspot-LEED pattern of the dark domain in a) acquired in the region highlighted by the red circle, showing that the misorientation angle $\boldsymbol{\theta}$ is 0˚.

4. DFT simulation of graphene moiré patterns

We discuss here in details the choice of the simulation cell for a given moiré structure, focusing in particular on the misorientation angles 0° and 11.3º. The simulation cell is defined by: (i) the periodicity (the smallest periodicity allowing to reasonably describe the real situation), and (ii) the relative registry between Ni(100) and graphene.

s-moiré

For the s-moiré, a first look at the experimental STM images reveals the absence of modulation along the [011] direction, suggesting a perfect matching of the unit cell of Ni(100) and the graphene zigzag periodicity in that direction, despite the small mismatch (≈1%) between the lattice parameters a_{gr} and a_{Ni} of graphene and Ni(100). The periodicity in the perpendicular direction, i.e., the $[01\bar{1}]$ crystallographic direction of Ni, is suggested by the observed

modulation along that direction and by geometrical consideration. The latter indicates that, considering an ideal, unbuckled graphene layer, the matching condition along the $[01\bar{1}]$ crystallographic direction of Ni is $n\sqrt{3}/2a_{gr} = m\ a_{Ni}$ (see figure S11). Approximate solutions can be found, neglecting the small mismatch between a_{gr} and a_{Ni}, the possible stretching of graphene in one direction and the buckling in the other. Once the periodicity of the supercell is chosen, the graphene is allowed to relax, and a certain buckling is actually found.

A reasonable choice is a Ni(100) (12×1) rectangular supercell, with the long side oriented along the $[01\bar{1}]$ crystallographic direction of Ni, containing 12 surface Ni atoms and 28 carbon atoms (see figures 3 and 4(a) of the main text). This supercell corresponds to 7 periodic units of graphene along the armchair direction. A lattice parameter of 2.49 Å and 2.46 Å has been considered for Ni(100) and graphene respectively, as in the reality, along the $[01\bar{1}]$ direction, while a common lattice parameter of 2.49 Å has been set along the [011] direction. In addition to the (12×1) model, a reduced model could be considered, described by a Ni(100) (7×1) rectangular supercell, with 7 surface Ni atoms and 16 carbon atoms, corresponding to 4 periodic units of graphene along the armchair direction. In this case each supercell contains only one beating. The agreement between the experimental and simulated STM is considerably worse than for the (12×1) supercell (see figure S12). Another possible choice is a (19×1) supercell, which contains 19 surface Ni atoms and 44 carbon atoms, corresponding to 11 periodic units of graphene along the armchair direction. Tests performed with such cell do not show significant improvements with respect to the less computationally expensive (12×1) supercell (see figure S12).

Once the periodicity of the moiré unit cell has been chosen, the optimal relative registry between graphene and Ni(100) has to be identified. For this purpose, we first consider the configuration with a line of carbon atoms along the zigzag chain perfectly on top of Ni atoms, and then we continuously slide the graphene along its zigzag direction, i.e., the [011] direction of Ni. For each configuration we calculate the final equilibrium structure allowing atomic relaxations perpendicular to the surface. The results are shown in figure S13, where the variation of the total

energy is calculated with respect to the initial registry (blue curve). The variation is small, but well beyond the relative numerical accuracy of our calculations. The minimum energy configuration (configuration C in figure S13) is the configuration that on average minimizes the C-Ni distances over the whole supercell, rather than the one with some C atoms perfectly on top of Ni (configurations A, E in figure S13). The simulated STM image shows remarkable similarity to the experimental one (figures 3(b,c)), indicating that the model can be used to explore the characteristics of graphene on a reasonable ground.

Finally, we found that the adsorption energy does not change shifting the graphene layer along its armchair direction, i.e., the $[01\bar{1}]$ direction of Ni, thus indicating an anisotropic graphene sliding (see figure S13, green curve).

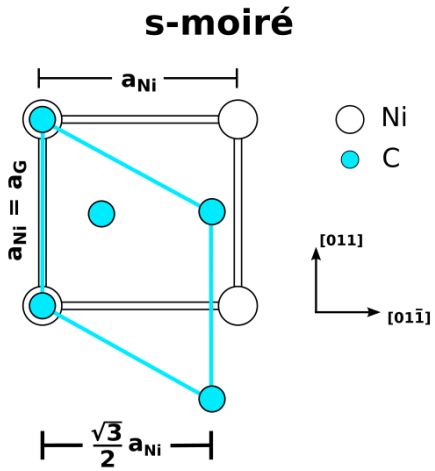

Figure S11 Schematic graph of the superposition of the Ni(100) square lattice and the graphene hexagonal lattice, when the zigzag chain of graphene is aligned with the crystallographic [011] direction of Ni.

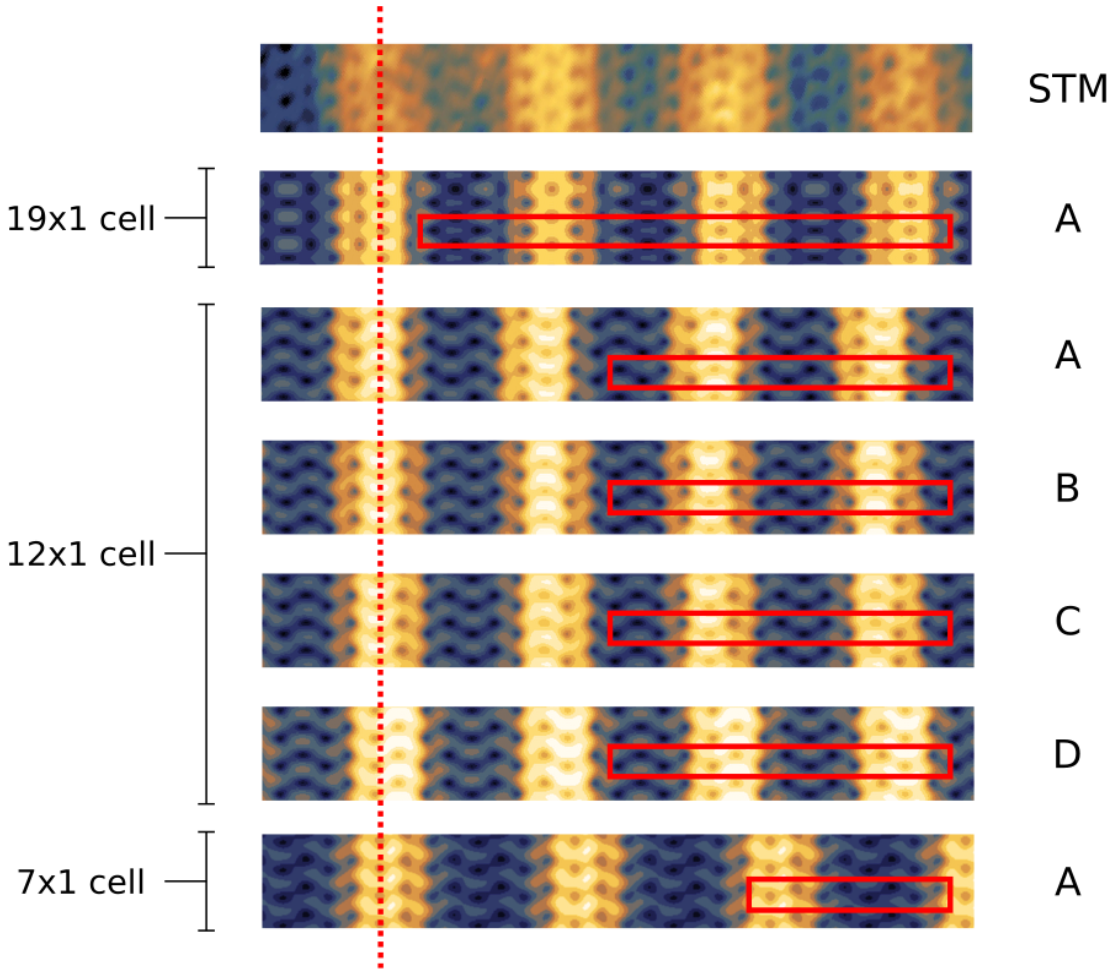

Figure S12 Comparison between experimental (STM) and simulated (19×1, 12×1, 7×1 cells) STM images for s-moiré: the simulation cells are highlighted. The dashed line is a guide to the eye in correspondence of the alignment of one bright region. **19×1 and 7×1 cells:** only the STM simulation of the configuration that maximizes the number of carbon atoms that are perfectly on-top with respect to nickel surface is reported (configuration A in figure S12). **12×1 cell:** the STM simulations of different configurations shifted along the [011] direction are reported (configurations A to D in figure S13 below).

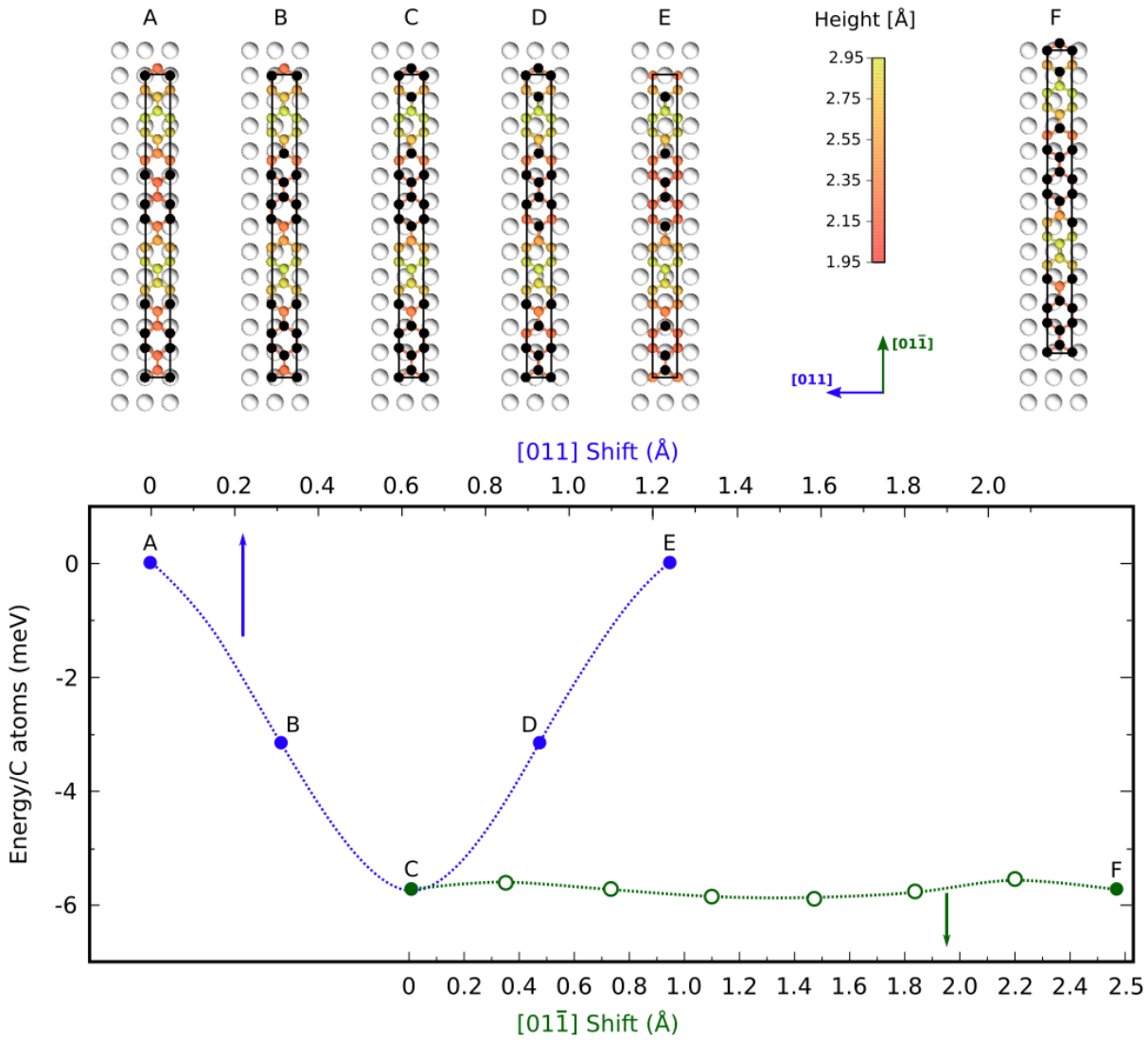

Figure S13 Top: Stick-and-ball models of the 12×1 cell for angle 0° moiré for different registry between Ni(100) and graphene. Top-left panels (A-E): graphene is shifted by displacements of 0.32 Å along the [011] direction; configuration E is equivalent to A although here represented with a different simulation cell. Top-right panel: final configuration of graphene progressively shifted from (C) along the [01$\bar{1}$] direction; configuration F is equivalent to C. **Bottom**: corresponding energies. Blue: shift along the [011] direction. Green: shift along the [01$\bar{1}$] direction by displacements of 0.36 Å.

n-moiré

The case of n-moiré is more complex. The choice of the simulation cell is even more arbitrary than for s-moiré, due to the absence of a clear common reference direction for the Ni(100) square lattice and for the graphene hexagonal lattice. We focus on a misorientation angle of 11.3°, where a convenient choice is a square cell, as indicated in figure S14.

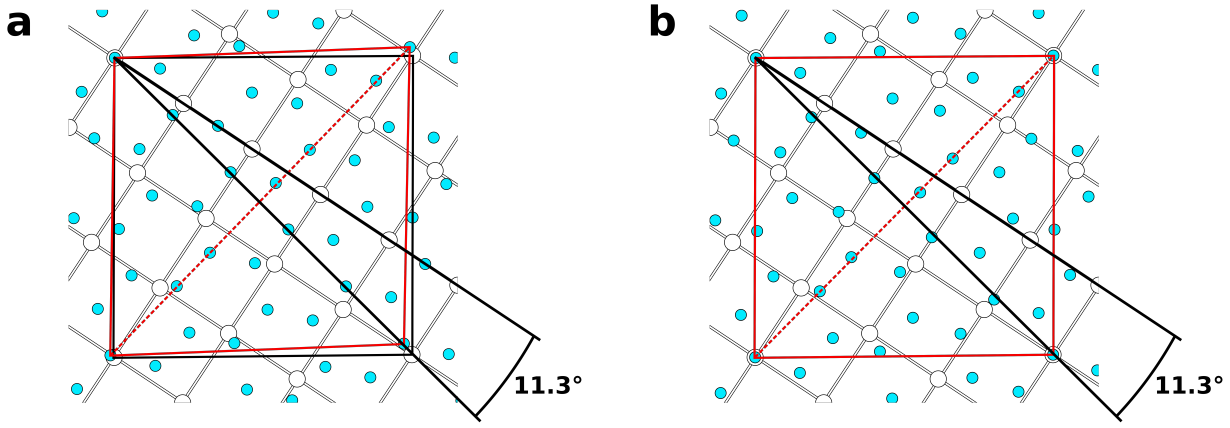

Figure S14 Sketch of the superposition of the ideal Ni(100) square lattice and the graphene hexagonal lattice with a misorientation angle of 11.3°, where one C atom of graphene is perfectly on-top of a surface Ni atom. (**a**): the graphene lattice is undistorted. The square drawn in black and the rhombus in red indicate possible choices of a repeated unit cell for Ni(100) lattice and graphene lattice, respectively, with very similar dimensions. We notice that the diagonals of the rhombohedral cell are very similar but not exactly equal: 9 a_{gr} the dashed one, and 5 $\sqrt{3}\, a_g$ the other. **(b)**: a small anisotropic distortion has been applied to the graphene lattice to transform the rhombohedral cell into the same square cell describing the Ni surface. The relative difference between the original lengths of the two diagonals of the rhombohedral graphene cell (about 4%) gives the order of magnitude of the strain applied to build the final model of the moiré cell. The coordinates of the C atoms internal to the cell have been properly rescaled by applying that strain, and a final optimization is obtained by DFT relaxation.

5. Graphene-Ni bonding

As explained in the main article, it is not possible to discriminate the contributions to the adsorption energy originating from each carbon atom. However, it is reasonable to qualitatively estimate the bond strength by the bond-order conservation rule: as the bonding with Ni surface atoms strengthens, the carbon-carbon bond weakens, resulting in a mild elongation of the carbon-carbon distance. This is evident in the s-moiré structure shown in figure S14(a), where the carbon-carbon distances are longer at valleys than at ridges of moiré regions.

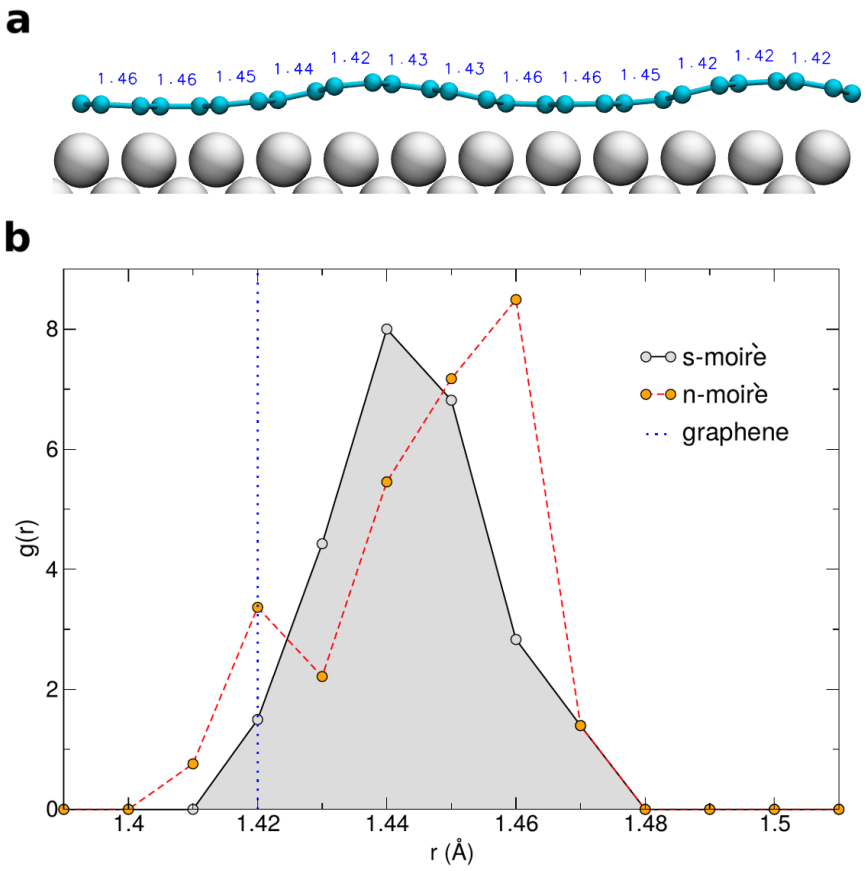

Figure S15: **(a)** Side view of the s-moiré structure. Several carbon-carbon distances are shown in Å. It becomes clear that distances at valleys are longer than at ridges. **(b)** Radial distribution function of carbon atoms of both moirés. Only distances corresponding to first neighbors are shown.

In order to compare the bond distances of both moirés, we show in figure S15(b) the radial distribution function of carbon atoms (g(r)) calculated for the corresponding relaxed DFT structures. This function can be interpreted as the number of carbon neighbors at a certain distance of each carbon atom, with respect to those in a random distribution of atoms. In the case of a pristine graphene, all first neighbors distances are 1.42 Å, so that the g(r) gives a sharp single peak. In both moirés, instead, a distribution of distances is found. Several values are above 1.42 Å, indicating a weakening of the carbon-carbon bond due to graphene chemisorption on the Ni surface. This effect is more pronounced in the n-moiré scenario where a larger right-shifting of g(r) with respect to that of pristine graphene is observed. Both the charge distribution and the radial distribution function of carbon atoms thus indicate that in the n-moiré structure most of the carbon atoms are chemisorbed to the metal surface, while in the s-moiré only those in the valleys are.

6. s-moiré: experimental evidence of differences in the electronic structure of ridge and valley regions

The morphological differences highlighted by STM between s-moiré ridge and valley regions, point to different graphene-substrate interactions, possibly affecting the electronic properties of the system, as predicted by DFT calculations that indicate graphene physisorption and chemisorption on the two regions, respectively. Experimental evidence of this interaction is not trivial to obtain and would require in any case a complex analysis and a detailed comparison with theory, which go beyond the scope of the present paper. However, preliminary scanning tunneling spectroscopy measurements (not shown) indicate significant differences in the electronic structure between the two regions.

Further evidence can be obtained by analyzing the exponential decay of the STM tunneling current I upon increasing the tip-surface distance d, reported in figure S16. As well known, the exponential decay goes as $I \propto e^{-2kd}$, where the decay constant k is, to a first approximation,

related to the local sample work function. Here, the exponential decay of the tunneling current was measured in open feedback-loop conditions while retracting the STM tip by 500 pm far from the sample surface, from an initial current setpoint of 0.5 nA (taken as zero distance). Several curves were measured on both ridge and valley regions, under identical experimental conditions. The decay constants were extracted by exponential fitting in the 0-100 pm range, where the logarithmic curves have a linear behaviour. This procedure yields values of the decay constants of 1.10 ± 0.01 $Å^{-1}$ for the ridge region and 0.98 ± 0.01 $Å^{-1}$ for the valley region for a +0.3 V bias between the sample and the tip.

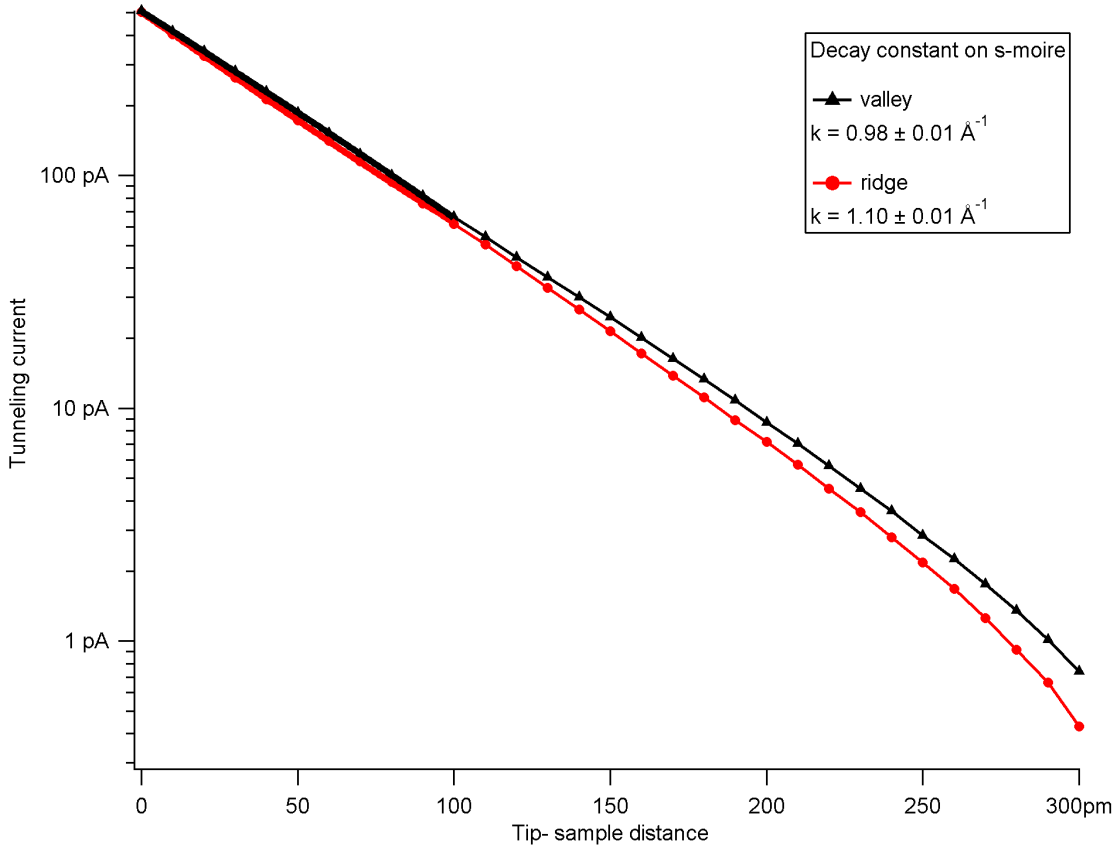

Figure S16: Decay of the tunneling current above valley (black) and ridge (red) regions, displayed on a logarithmic scale. The exponential fitting was performed in the 0-100 pm range. A higher decay constant on the ridge region is evident.

The theoretical values of the decay constant are obtained from the variation of the energy-integrated density of states (ILDOS) along lines perpendicular to the surface increasing the distance from graphene, taken as zero setpoint. The calculated decay constants for the physisorbed (ridge) and the chemisorbed (valley) regions are 1.28 ± 0.02 Å^{-1} and 1.18 ± 0.02 Å^{-1}, respectively, using the same bias of +0.3 V. These values are in good agreement with the experimental ones; in particular the measured and calculated relative difference between the two decay constants is almost identical, strengthening the validity of our theoretical description of the system.